Ceramics International 42 (2016) 8170–8178

Contents lists available at ScienceDirect

Ceramics International

journal homepage: www.elsevier.com/locate/ceramint

# The formation of feldspar strontian ($SrAl_2Si_2O_8$) via ceramic route: Reaction mechanism, kinetics and thermodynamics of the process

Petr Ptáček*, František Šoukal, Tomáš Opravil, Eva Bartoníčková, Jaromír Wasserbauer

*Brno University of Technology, Faculty of Chemistry, Centre for Materials Research CZ.1.05/2.1.00/01.0012, Purkyňova 464/118, Brno CZ-612 00, Czech Republic*

ARTICLE INFO

*Article history:*
Received 12 January 2016
Received in revised form
2 February 2016
Accepted 3 February 2016
Available online 10 February 2016

*Keywords:*
Strontian
Sr-celsian
Feldspar
Ceramic
Sr-gehlenite
Kinetics

ABSTRACT

The reaction mechanism, the equilibrium composition, the temperature range of stability of formed intermediates as well as the kinetics and thermodynamics of activated state during the formation of monoclinic strontium-aluminum-silicate feldspar stroncian ($SrAl_2Si_2O_8$) via the ceramic route from the mixture of $SrCO_3$, $Al_2O_3$ and $SiO_2$ is described in this work. Strontian does not appear up to the temperature of 1150 °C and is the only stable phase at the temperature ≥1600 °C. Three independent reactions lead to two parallel reaction pathways, i.e. the formation of strontian from single or binary oxides (1) and with Sr-gehlenite as the intermediate (2). Since the reaction rate constants ratio is higher than one ($k_1/k_2 > 1$), the first reaction route is favored according to the Wegscheider principle. The kinetics of chemical reaction of 1.5 order corresponding to the kinetic function $F_{2/3}$ ($(1-\alpha)^{-1/2}-1$) was determined as the rate determining the mechanism of formation of strontian. The integral and differential methods show that the process requires average apparent activation energy of 229.3 kJ $mol^{-1}$. The determined average value of frequency factor is $2.1 \times 10^5$ $s^{-1}$.



## 1. Introduction

Since alumosilicate feldspars of fundamental formula $MT_4O_8$ (or $M_xT_yO_8$, where $y$ reaches 4 and the parameter $x$ does not fall below 0.975 [1]) are the most abundant minerals in the Earth's crust [2], these tectosilicates [3] are investigated due to the importance of their petrography [4,5], understanding of Earth's geology [5,6] and industrial importance in glass industry and production of ceramics [7–10]. **T**-sites are occupied by small strongly charged cations (typically $Si^{4+}$ and $Al^{3+}$) and **M**-sites are occupied by larger weakly charged cati`ons. Feldspars can be characterized by the content of all 92 naturally occurring elements [1]. Weathering and hydrothermal change of feldspar leads to the formation of minerals such as kaolinite [11,12], montmorillonite [13], illite [14] or mixed-layer clay minerals [15].

The feldspar crystal structure is composed of a 3D framework of corner-shared tetrahedra which are centered by $Si^{4+}$ ($Ge^{4+}$) and $Al^{3+}$ ($Ga^{3+}$). Large alkali ($Na^+$, $K^+$) or alkaline-earth ions ($Ca^{2+}$, $Sr^{2+}$, $Ba^{2+}$) in the interstices balance the charge caused by different charges of tetrahedral $Al^{3+}$ ($Ga^{3+}$) and $Si^{4+}$ ($Ge^{4+}$) ions. Feldspars with smaller cations ($Na^+$, $Ca^{2+}$) are triclinic, whereas larger cations ($Sr^{2+}$, $Ba^{2+}$) tend to support the monoclinic symmetry. Feldspars are known to undergo several phase transitions, which are of the order–disorder or displacive type. $MeAl_2Si_2O_8$ (Me = Ca, Sr, Ba) feldspars remain essentially ordered at all temperatures below the melting point [2,16–18].

Similar to anorthite ($CaAl_2Si_2O_8$, [19–22]), barium feldspar celsian ($BaAl_2Si_2O_8$, BAS) and strontium feldspar strontian ($SrAl_2Si_2O_8$, SAS, Fig. 1(a–c)) are the materials of great technological interest due to low thermal expansion coefficient ($2.29 \times 10^{-6}$ $°C^{-1}$ for BAS [23] and $2.5 \times 10^{-6}$ $°C^{-1}$ for SAS [24,25]), low and thermally stable dielectric constant, low dielectric losses, high mechanical strength, chemical inertness, and high melting temperature (1760 °C for BAS [2,23,26] and 1650 °C for SAS [23,27,28]), therefore are known as materials for the matrix of fiber-reinforced ceramic composites, protective coatings, electro-ceramics and refractories [23,28–34]. Other significant applications include the preparation of glass ceramics [23,35–37] and luminescent pigments of $XAl_2Si_2O_8:M^{n+}$ (where X = Ca, Sr, Ba and $M^{n+}$ denotes ions of doped element) [38–44].

The strontium aluminate polymorphs of SAS are monocelsian (SM) and hexacelsian (SP). Sr-hexacelsian is known only as the synthetic product and Sr-monocelsian occurs as the mineral slawsonite ($P2_1/a$) [23,25,45]. The reversible SM↔SP transformation within the temperature range from 600 to 800 °C causes volume changes of approximately 3% [24,25,28]. Celsian and Sr-celsian give rise to solid

* Corresponding author. Tel.: +420 541 149 389.
*E-mail addresses:* ptacek@fch.vutbr.cz (P. Ptáček), soukal@fch.vutbr.cz (F. Šoukal), opravil@fch.vutbr.cz (T. Opravil), bartonickova@fch.vutbr.cz (E. Bartoníčková), wasserbauer@fch.vutbr.cz (J. Wasserbauer).

http://dx.doi.org/10.1016/j.ceramint.2016.02.024

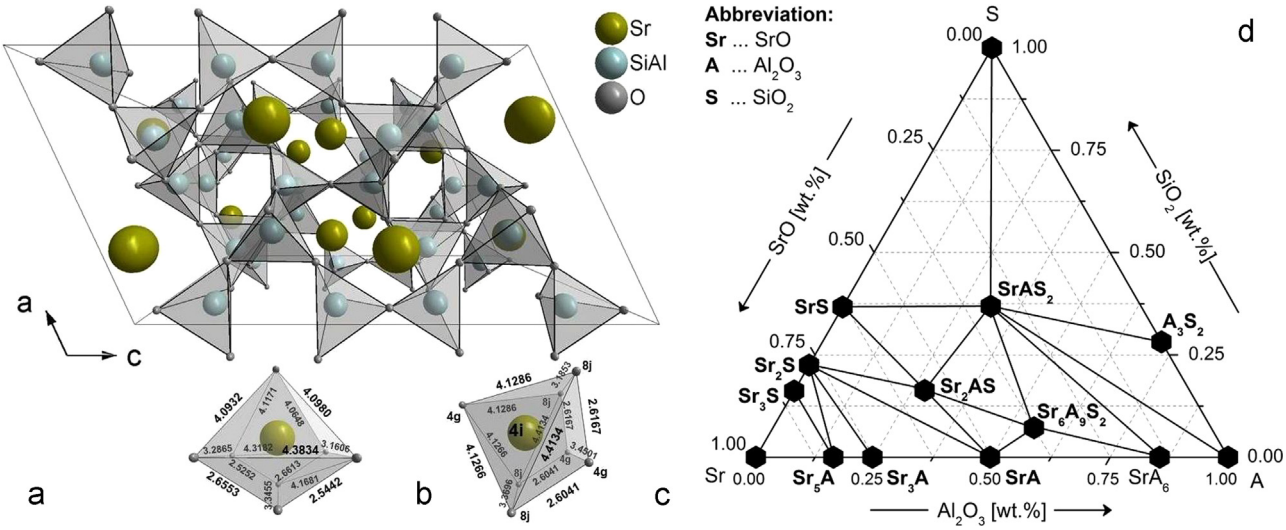


**Fig. 1.** Structure of strontian in perspective view along the *b*-axis according to Chiari et al. [48] (a), displayed with Sr polyhedron (b), Sr polyhedron according to Grundy and Ito [47] (c) and phase relationships for the system $SrO-Al_2O_3-SiO_2$ at the temperature of 1350 °C according to Dear [49] (d).

solutions, $(Ba,Sr)Al_2Si_2O_8$, over the whole composition range of binary phase diagram $BaAl_2Si_2O_8-SrAl_2Si_2O_8$ [28,30]. Therefore strontium aluminum silicate feldspar is isostructural with celsian and due to similar polymorphism, strontian is termed in many papers [23,28–30,46] as Sr-celsian.

The crystal structures of non-stoichiometric and partially disordered monoclinic strontium feldspar were described by Grundy and Ito [47] and Chiari et al. [48], respectively. While Grundy and Ito [47] refined the highly disordered structure (**C2/M** symmetry), a more highly ordered Al/Si arrangement with the space group **I2/c** (Fig. 1) was reported by Chiari et al. [48]. The cell parameters are $a=8.388$, $b=12.974$, $c=14.263$ Å and $\beta=115.2°$.

Sr-celsian or its solid solutions with celsian or anorthite are usually prepared via solid-state synthesis from the mixture of oxides and carbonates [2,40,45,50] or using mechanically activated precursor mixture [51]. The following equation can be used in the case of pure celsian:

$$SrCO_3 + Al_2O_3 + 2SiO_2 \rightarrow SrO{\cdot}Al_2O_3{\cdot}2SiO_2 + CO_2(g) \quad (1)$$

The process is more complex due to the formation of various intermediates such as Sr-silicates ($SrSiO_3$ and $SrSi_2O_4$), strontium aluminates ($Sr_3Al_2O_6$, $SrAl_2O_4$) and mullite ($Al_6Si_2O_3$) [45]. Another reported synthesis uses a blend of kaolinite and $SrCO_3$ [29]

$$SrCO_3 + Al_2O_3{\cdot}2SiO_2{\cdot}2H_2O \rightarrow SrO{\cdot}Al_2O_3{\cdot}2SiO_2 + CO_2(g) + 2H_2O(g) \quad (2)$$

The sub-solidus compatibility relationships between binary and ternary phases in the $SrO-Al_2O_3-SiO_2$ system at the temperature of 1350 °C (Fig. 1(d)) were calculated by Dear [29]. Small quantities of $H_3BO_3$ can also be used as the flux agent [41,42]. Moreover, the preparation of Sr-celsian by thermal treatment of Ba-, Sr-exchanged zeolite A was described. Usual sequence of thermal transformations includes zeolite→amorphous phase→HC→MC [28,30,36,46,52,53]. Other described preparation techniques include the sol–gel process [33,35,54], the coprecipitation method [43], the mechanochemical activation [55], the combustion method [44], the hydrothermal [56] and microwave assisted hydrothermal synthesis [57].

The reaction mechanism, kinetics and thermodynamics of activated state of formation of feldspar strontian were investigated in this work via the reaction model dependent technique using the integral and differential methods. The course of synthesis was investigated by thermal analysis, X-ray diffraction analysis, heating microscopy and electron microscopy in order to determine the main reaction pathway.

## 2. Experimental

### 2.1. Synthesis and analysis of sample properties

The raw meal for the synthesis of strontian was prepared by mixing of strontium carbonate ($SrCO_3$), aluminum oxide ($Al_2O_3$) and silica ($SiO_2$) in the mass ratio of 1.45:1:1.18 which corresponds to the stoichiometric composition of $SrAl_2Si_2O_8$ (Eq. (1) and Fig. 1(b)). Initial homogenization of raw meal was performed by short milling (5 min) in vibration laboratory mill. The influence of temperature on the properties of sintered ceramic body was determined on disc with the diameter of 35 mm prepared by pressing of 10 g of raw meal under the pressure of 25 MPa. The specimens were then treated to the temperatures of 1200, 1300, 1400, 1500 and 1600 °C under the rate of 2 °C $min^{-1}$.

The course of synthesis of strontian during the thermal treatment of raw meal was investigated by TG-DTA (TG-DTA analyzer SDT Q600). A amount of 30 mg of sample were heated in air conditions (100 $cm^3$ $min^{-1}$) under the rate of 10 °C $min^{-1}$. The furnace was connected with the measuring cell (TGA/FT-IR Interface, Thermo Scientific) equipped with infrared spectrometer (iS 10, Thermo Scientific) where the composition of gas phase (EGA) was investigated. Heating microscopy (EM 201, Leitz) was used to determine the behavior of specimen during the sintering. The changes in the phase composition during the thermal treatment were evaluated by high temperature X-ray analysis (XRD, X´Petr Empyrean, PANanalytical with Cu(Kα) radiation at 40 kV and the current of 30 mA applying high temperature chamber HTK 16, Anton Paar). Scanning electron microscopy with EDX (SEM, Zeis EVO LS10 with W-cathode) was used for the analysis of sample after the thermal treatment. HSC v.7.1 software was used for the estimation of the independent reaction thermodynamics.

### 2.2. Mechanism, kinetics and thermodynamics of synthesis

The kinetics of formation of feldspar stroncian was evaluated via the non-isothermal model (kinetic function)-fitting integral technique based on the Coats–Redfern equation [58,59]

$$\ln\left[\frac{g(\alpha)}{T^2}\right] = \ln\left[\frac{A\,R}{\Theta\,E_{ap}} - \left(1 - \frac{2\,RT}{E_{ap}}\right)\right] - \frac{E_a}{RT} \cong \ln\left[\frac{A\,R}{\Theta\,E_{ap}}\right] - \frac{E_a}{RT} \quad (3)$$

where $E_{ap}$ is the apparent activation energy, $A$ is the frequency (pre-exponential) factor, and $g(\alpha)$ represents the kinetic functions (the overview of $g(\alpha)$ is listed in the following literature

[58,60–71] and Table 3). The plot of $\ln(g(\alpha)/T)$ versus $T^{-1}$ gives straight line ($R^2 \rightarrow 1$) with the slope $-E_{ap}/R$ for the suitable choice of $g(\alpha)$. The intercept with $y$-axis ($\ln[AR/\Theta E_{ap}]$) enables then to calculate the value of frequency factor ($A$). The results were verified by the differential method based logarithmic form of generalized equation [72]

$$\ln\left[\frac{d\,\alpha/d\,t}{f(\alpha)}\right] = \ln\left[\frac{A}{\Theta}\right] - \frac{E_a}{RT} \quad (4)$$

The plot of $\ln[d\alpha/dt\ /f(\alpha)]$ versus $T^{-1}$ gives straight line for proper $f(\alpha)$ function (Table 3).

## 3. Results and discussion

### 3.1. Investigation of behavior of raw meal upon thermal treatment

The HT-XRD plot in Fig. 2(a) shows the changes in phase composition during the thermal treatment of raw meal. The shift in quartz diffraction is caused by the transformation of low-quartz ($\alpha$) to high-quartz ($\beta$) at the temperature of 575 °C. This reversible displacive (athermal) transition is deeply discussed in the following literature [73–75]. The diffraction lines of strontium carbonate disappear within the temperature range from 775 to 850 °C. In the same temperature interval the maximum intensity of diffraction lines of strontium oxide was reached. The amount of SrO then decreases with the formation of tristrontium aluminate ($Sr_3Al_2O_5$). With increasing temperature, tristrontium aluminate reacts with alumina to hexagonal strontium aluminate. The features of $Sr_3A$ and SrO disappear at the temperature of 1125 °C.

The formation of strontium orthosilicate ($SrSiO_4$) at the temperature of 775 °C is responsible for decreasing intensity of diffraction lines of $SiO_2$. At the temperature of 900 °C the features of strontium metasilicate appear. The diffraction lines of this phase increase with increasing temperature, while the intensity of diffraction lines of $Sr_2SiO_4$ decreases. The features of strontian appear at the temperature of 1150 °C. As the intensity of diffraction lines of feldspar increases with increasing temperature, the intensity of other components decreases (Fig. 2(b)). The evolution of phase composition of specimen during the thermal treatment to the temperature of 1660 °C is shown in Fig. 6(a).

The typical TG-DTA and heating microscopy plot is shown in Fig. 3. These results were supplemented by the results of EGA analysis (Fig. 4). The first endothermic effect at the temperature of 92 °C is accompanied by increasing intensity of $CO_2$ and $H_2O$ on EGA. Drying, desorption of carbon dioxide and the first dehydration step of $Sr(OH)_2 \cdot 8H_2O$ (formed via adsorption of air humidity on the recently formed surface of treated (milled) raw meal) to $Sr(OH)_2 \cdot 6H_2O$ [76] decreases the mass of sample by 0.06%. The second (formation of $Sr(OH)_2 \cdot H_2O$ [76]) and final dehydration step to $Sr(OH)_2$ shows a small endothermic peak at 180 °C. The both stages can be recognized on DTG at temperature of 170 and 210 °C. Polymorphic transformation of $\beta$-$Sr(OH)_2$ to $\alpha$-$Sr(OH)_2$ shows a small endothermic peak at the temperature of 305 °C. Melting and decomposition of $Sr(OH)_2$ takes place in the temperature range from 430 to 645 °C. The process shows peak temperature of 605 °C and mass of sample was reduced of 1.01%. The released water and its autodissociation in the hydroxide flux ($2OH^- \leftrightarrow H_2O + O^{2-}$, where water acts as a strong acid [77]) is followed by the reaction of melt with $SrCO_3$ and the increase of intensity of $CO_2$ and $H_2O$ on EGA (Fig. 4).

Sharp endothermic peak at the temperature of 573 °C is caused by displacive transition between low ($\alpha$)- and high ($\beta$)-quartz polymorphs (see Fig. 2). The endothermic nature of this transition slows down the reaction of molten phase with strontium carbonate, i.e. depression of the concentration of $CO_2$ on EGA has appeared (Fig. 4). The concentration of water vapor is increasing in the same time.

The thermal decomposition of strontium carbonate reduces the mass of sample by 11.2% within the temperature range from 685 to 1010 °C. The process increases the response of $CO_2$ on EGA (Fig. 4). The shape of peak caused by observed effects is affected by the transformation of orthorhombic ($\alpha$-$SrCO_3$) to hexagonal ($\beta$) polymorph. The kinetics and the mechanism of this process were described in previous work [78]. The results of heating microscopy show that the specimen area increases by ~5% in the temperature interval limited by polymorphic transformation of $SrCO_3$ and the occurrence of strontian. The small endothermic peak at the temperature of 1160 °C indicates the formation of melt from which primary strontian starts crystallizing. The exothermic nature of crystallization process then leads to the exothermic peak at 1195 °C.

Other peaks appears the consequence of establishing of equilibrium composition, i.e. the formation of strontian as the single phase via reactions between the different intermediates (see Eq. (9)) and intermediates with single oxides (Eqs. (8) and (9)). The establishment of equilibrium composition leads to the formation of secondary strontian. The reaction mechanism of formation is different, but no structural difference between primary and secondary formed strontian is observed. According to the results of heating microscopy (Fig. 3(b)), the strontian starts to melt at the temperature of 1660 °C.

The scanning electron microscopy results of raw meal treated to temperatures marked in Fig. 3(b) are shown in Fig. 5. The results of HT-XRD (Fig. 2) indicate that the diffraction lines of strontian appear at the temperature of 1150 °C. The SEM analysis of sample treated to this temperature (a) shows the growth of nuclei of strontian. At the temperature of 1300 °C (b) the plate-like particles of strontian can be recognized. The structure consists of many narrow layers of twinned feldspar crystals (multiple lamellar [010] contact twins according to the "*albite law*" [79,80]), which endow the parts of the crystal with faintly striped appearance. The melt formed with increasing temperature enables the recrystallization and growth of large plate-like particles of tertiary strontian (c and d) which are stable up to the melting temperature. The process is accompanied by the expansion of specimen (see Fig. 3(b)).

**Table 1**
The derivation of ratio of rate constants for the formation of strontian ($k_1$) and Sr-gehlenite ($k_2$).

| | | | | | |
|---|---|---|---|---|---|
| Temperature | [°C] | 1150 | 1300 | 1400 | 1450 |
| Strontian | [%] | 4 | 36 | 69 | 83 |
| Sr-gehlenite | [%] | 0 | 6 | 7 | 0 |
| $\boldsymbol{k_1/k_2 = w_1/w_2 > 1}$ | | – | 6 | 9.9 | – |

**Table 2**
Reaction thermodynamics for independent reactions Eqs. ((8)–10).

| **Temperature [°C]** | 1150 | 1200 | 1300 | 1400 | 1500 | 1600 |
|---|---|---|---|---|---|---|
| **Equation** | $\Delta_r G°$ [kJ mol$^{-1}$] | | | | | |
| **Eq.** (8) | −3.017 | −2.973 | −2.806 | −2.534 | −2.161 | −1.693 |
| **Eq.** (9) | −42.214 | −42.335 | −42.517 | −42.626 | −42.670 | −42.659 |
| **Eq.** (10) | −25.872 | −24.907 | −23.034 | −21.225 | −19.463 | −17.729 |

**Table 3**
The overview of results with applied kinetic functions [59,82–87] and the evaluation of the most probable reaction mechanism (marked by bold) for the formation of strontian.

| Abr. | Kinetic function | | Description | | n | $R^2$ | |
|---|---|---|---|---|---|---|---|
| | $g(\alpha)=kt$ | $f(\alpha)=k^{-d\alpha/dt}$ | | | | Int. | Diff. |
| $F_{1/3}$ | $1-(1-\alpha)^{2/3}$ | $(3/2)(1-\alpha)^{1/3}$ | Chemical process or mechanism non-invoking equations | One-third order | 1/3 | 0.9482 | 0.4472 |
| $F_{3/4}$ | $1-(1-\alpha)^{1/4}$ | $4(1-\alpha)^{3/4}$ | | Three-quarters order | 3/4 | 0.9774 | 0.8948 |
| $F_{2/3}$ | $(1-\alpha)^{-1/2}-1$ | $2(1-\alpha)^{3/2}$ | | One and half order | 1+1/2 | 0.9998 | **0.9997** |
| $F_2$ | $(1-\alpha)^{-1}-1$ | $(1-\alpha)^2$ | | Second order | 2 | 0.9961 | 0.9903 |
| $F_3$ | $(1-\alpha)^{-2}-1$ | $(1/2)\ (1-\alpha)^3$ | | Third order | 3 | 0.9706 | 0.9647 |
| $P_{3/2}$ | $\alpha^{3/2}$ | $(2/3)\alpha^{-1/2}$ | Acceleratory rate equations[a] | Mampel's power law | | 0.9288 | 0.4271 |
| $P_{1/2}$ | $\alpha^{1/2}$ | $2\alpha^{1/2}$ | | | 2 | 0.8701 | 0.5297 |
| $P_{1/3}$ | $\alpha^{1/3}$ | $3\alpha^{2/3}$ | | | 3 | 0.7759 | 0.7199 |
| $P_{1/4}$ | $\alpha^{1/4}$ | $4\alpha^{3/4}$ | | | 4 | 0.5752 | 0.7859 |
| $E_1$ | $\ln\alpha$ | $\alpha$ | | Exponential law | | 0.9660 | 0.9050 |
| $A_1$, $F_1$ | $-\ln(1-\alpha)$[b] | $(1-\alpha)$ | Sigmoidal rate equations or random nucleation and subsequent growth | Kolmogorov–Johnson–Mehl–Avrami– Erofeev equation[c] | 1 | 0.9892 | 0.9712 |
| $A_{2/3}$ | $-\ln(1-\alpha)^{2/3}$ | $2/3(1-\alpha)[-\ln(1-\alpha)]^{1/3}$ | | | 1.5 | 0.9870 | 0.9385 |
| $A_2$ | $-\ln(1-\alpha)^{1/2}$ | $2(1-\alpha)[-\ln(1-\alpha)]^{1/2}$ | | | 2 | 0.9841 | 0.8663 |
| $A_3$ | $-\ln(1-\alpha)^{1/3}$ | $3(1-\alpha)[-\ln(1-\alpha)]^{2/3}$ | | | 3 | 0.9755 | 0.3516 |
| $A_4$ | $-\ln(1-\alpha)^{1/4}$ | $4(1-\alpha)[-\ln(1-\alpha)]^{3/4}$ | | | 4 | 0.9774 | 0.1435 |
| $A_u$ | $\ln(\alpha/(1-\alpha))$ | $\alpha(1-\alpha)$ | | Prout–Tomkins equation[d] | | – | 0.0016 |
| $R_1$, $F_0$, $P_1$ | $\alpha$ | $(1-\alpha)^0$ | Deceleratory rate equations based on boundary reactions | Contracting disk | | 0.9182 | 0.0109 |
| $R_2$, $F_{1/2}$ | $1-(1-\alpha)^{1/2}$ | $2(1-\alpha)^{1/2}$ | | Contracting cylinder | 2 | 0.9182 | 0.6923 |
| $R_3$, $F_{2/3}$ | $1-(1-\alpha)^{1/3}$ | $2(1-\alpha)^{2/3}$ | | Contracting sphere | 3 | 0.9724 | 0.8464 |
| $D_1$ | $\alpha^2$ | $1/2\alpha$ | Deceleratory rate equations: based on diffusion mechanism | Parabolic rate law[e] | | 0.9334 | 0.9050 |
| $D_2$ | $\alpha+(1-\alpha)\ln(1-\alpha)$ | $[-\ln(1-\alpha)]^{-1}$ | | Valensi equation[f] | | 0.8182 | 0.8368 |
| $D_3$ | $(1-(1-\alpha)^{1/3})^2$ | $3/2(1-\alpha)^{2/3}[1-(1-\alpha)^{1/3}]^{-1}$ | | Jander equation[g] | | 0.9195 | 0.9483 |
| $D_4$ | $1-(2\alpha/3)-(1-\alpha)^{2/3}$ | $3/2[(1-\alpha)^{-1/3}-1]^{-1}$ | | (C)G-B equation[h] | | 0.9635 | 0.8887 |
| $D_5$ | $((1-\alpha)^{-1/3}-1)^2$ | $3/2(1-\alpha)^{4/3}[(1-\alpha)^{-1/3}-1]^{-1}$ | | ZLT equation[i] | | 0.9985 | 0.9990 |
| $D_6$ | $((1+\alpha)^{1/3}-1)^2$ | $3/2(1+\alpha)^{2/3}[(1+\alpha)^{1/3}-1]^{-1}$ | | Anti-Jander equation [84] | | 0.9192 | 0.4172 |
| $D_7$ | $1+(2\alpha/3)-(1+\alpha)^{2/3}$ | $3/2[(1+\alpha)^{-1/3}-1]^{-1}$ | | Anti-GB equation [85] | | 0.9241 | – |
| $D_8$ | $((1+\alpha)^{-1/3}\ -1)^2$ | $3/2(1+\alpha)^{4/3}[(1+\alpha)^{-1/3}-1]^{-1}$ | | Anti-ZLT equation[i] | | 0.9025 | – |
| $G_1$ | $1/2(1-\alpha)$ | $1-(1-\alpha)^2$ | Another kinetics equations with unjustified mechanism | | | 0.8098 | 0.8701 |
| $G_2$ | $1/3(1-\alpha)^2$ | $1-(1-\alpha)^3$ | | | | 0.6945 | 0.7952 |
| $G_3$ | $1/4(1-\alpha)^3$ | $1-(1-\alpha)^4$ | | | | 0.5799 | 0.6868 |
| $G_4$ | $1/2(1-\alpha)[-\ln(1-\alpha)]^{-1}$ | $[-\ln(1-\alpha)]^2$ | | | | 0.9910 | 0.9859 |
| $G_5$ | $1/3(1-\alpha)[-\ln(1-\alpha)]^{-2}$ | $[-\ln(1-\alpha)]^3$ | | | | 0.9915 | 0.9971 |
| $G_6$ | $1/4(1-\alpha)[-\ln(1-\alpha)]^{-3}$ | $[-\ln(1-\alpha)]^4$ | | | | 0.9918 | 0.9995 |
| $G_7$ | $4\{(1-\alpha)[1-(1-\alpha)]^{1/2}\}^{1/2}$ | $[1-(1-\alpha)^{1/2}]^{1/2}$ | | | | 0.9413 | 0.5890 |
| $G_8$ | $6\{(1-\alpha)^{2/3}[1-(1-\alpha)]^{1/3}\}^{1/2}$ | $[1-(1-\alpha)^{1/3}]^{1/2}$ | | | | 0.9588 | 0.6065 |

[a] The rate-determining step is the nucleation of new phase.
[b] The equation is also termed as the first order Mampel law.
[c] The general equation of this model is $kt=[-\ln(1-\alpha)]^{1/n}$ and then $\alpha=1-\exp(-kt^n)$.
[d] The equation $(\ln(\alpha/(1-\alpha))=k(t-t_{1/2}))$ is based on the assumption of linearly growing nuclei branching into chains.
[e] The Wagner's parabolic rate law: $\alpha^2=2kt$, where the rate of diffusion slows down with increasing thickness of product layer (frequently observed during the oxidation of metals [64]).
[f] Valensi used Fick's first diffusion law to express the kinetics of diffusion through spherical and cylindrical shell [86].
[g] The process is controlled by the diffusion through nonporous layer of product of spherical geometry [86,87].
[h] Crank, Ginstling, and Braunshtein's equation [86,88].
[i] Zhuravlev, Lesotkin and Tempelman [68].

### 3.2. Investigation of reaction mechanism

The course of synthesis during the thermal treatment of raw meal, the temperature range of stability of formed intermediates, their further reactions and the formation of feldspar strontian are schematically drawn in Fig. 6(a). The main reaction pathway is initiated by thermal decomposition of $SrCO_3$. The surplus of SrO on the reaction interface with particles of $SiO_2$ and $Al_2O_3$ leads to the formation of $Sr_3Al_3O_6$ and $Sr_2SiO_4$ at first, but with increasing temperature $SrAl_2O_4$ and $SrSiO_3$ prevail. Feldspar strontian firstly appears at the temperature of 1150 °C.

Within the temperature range from 1250 to 1425 °C, the product of thermal treatment contains Sr-gehlenite ($Sr_2Al_2SiO_7$) as well. That means that the relationship between Sr-gehlenite and celsian is probably not the same like that of gehlenite ($Ca_2Al_2SiO_7$) and anorthite ($CaAl_2Si_2O_8$), where anorthite is formed from gehlenite [20,22]. The formation of Sr-gehlenite is probably caused by the lack of $SiO_2$ in the reaction zone and by the site saturation of strontium.

These results (Fig. 6(a)) indicate that the formation of strontian and Sr-gehlenite should be considered as parallel (competing) reactions of the same order, with the rate constants $k_1$ and $k_2$, respectively. Increasing temperature supports the rate of diffusion of $SiO_2$ to the reaction zone and Sr-gehlenite is next transformed to strontian ($k_3$). Under isothermal conditions, the formation of $Sr_2Al_2SiO_7$ and its further transformation to $SrAl_2Si_2O_8$ are sequential reactions. Strontian remains a stable phase from the temperature of 1150 to the melting temperature of 1660 °C and quantitative X-ray diffraction analysis shows, that the concentration ratio of strontian ($w_1$) to gehlenite ($w_2$) is higher than one (Table 1). From that the reaction rate constant of formation of strontian being higher than that of gehlenite ($k_1 > k_2$) can be estimated (Wegscheider principle [81]).

The system contains six compounds ($N=6$; $Al_2O_3$, $SiO_2$, $SrAl_2O_4$, $SrSiO_3$, $Sr_2Al_2SiO_7$ and $SrAl_2Si_2O_8$) at the temperature of 1350 °C which are formed from four elements ($M=4$; Sr, Al, Si and O). The number and the stoichiometry of independent chemical reactions were solved using the phase diagram and the Gibbs stoichiometric rule [82,83]

$$R = N - h \quad (5)$$

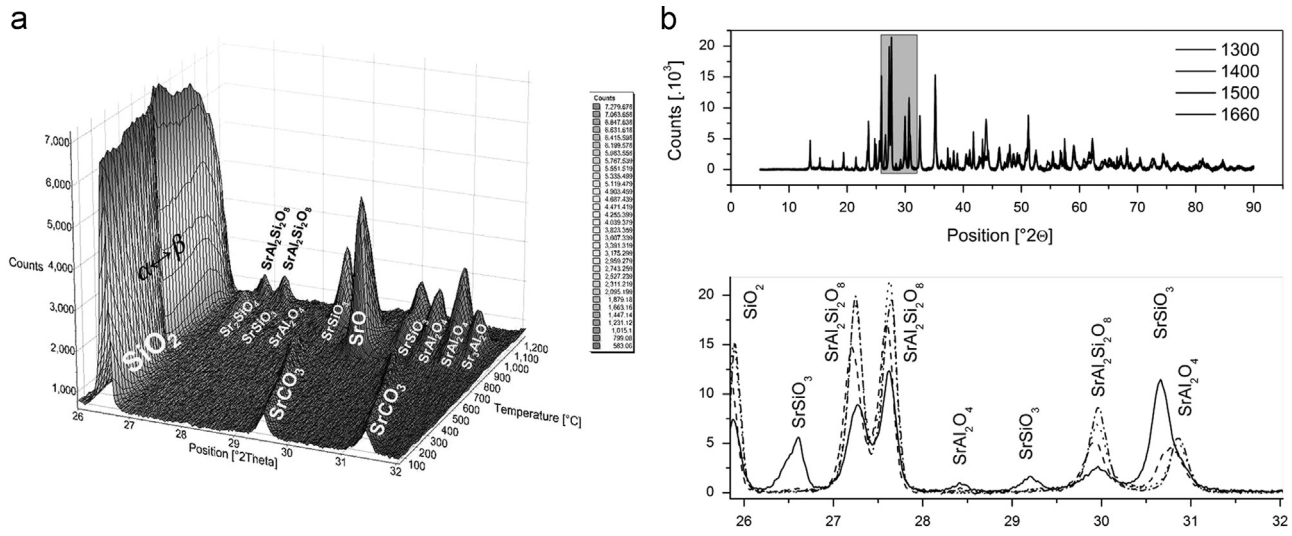


**Fig. 2.** High-temperature X-ray diffraction analysis of raw meal during the thermal treatment to 1250 °C (a) and X-ray diffraction patterns of sample treated to the temperatures of 1300, 1400, 1500 and 1660 °C (b).

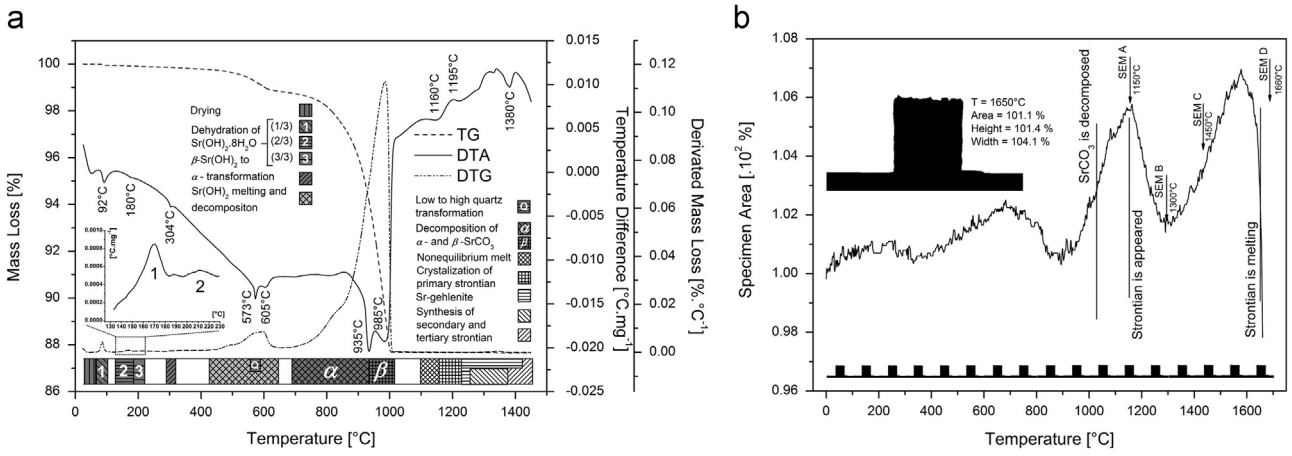


**Fig. 3.** Thermal analysis of raw meal during the thermal treatment to the temperature of 1450 °C: TG-DTA (a) and heating microscopy (b).

where the rank ($h$) of matrix of constitution coefficients ($A$) has the value of 3 (Eq. (6)).

$$\begin{vmatrix} 1 & 2 & 1 & 0 & 1 & 0 \\ 2 & 2 & 2 & 0 & 0 & 2 \\ 2 & 1 & 0 & 1 & 1 & 0 \\ 8 & 7 & 4 & 2 & 3 & 3 \end{vmatrix} = \cdots = \begin{vmatrix} 1 & 0 & 1 & 0 & -1 & 2 \\ 0 & 1 & 0 & 0 & 1 & -1 \\ 0 & 0 & 1 & -\frac{1}{2} & -1 & \frac{3}{2} \end{vmatrix} \quad \Rightarrow \quad h = 3 \tag{6}$$

According to Eq. (5) there are three independent reactions in the system, the stoichiometry of which can be derived via calculation of stoichiometric coefficients ($\nu$) from the relations

$$A\nu = 0 \Rightarrow \begin{vmatrix} 1 & 0 & 1 & 0 & -1 & 2 \\ 0 & 1 & 0 & 0 & 1 & -1 \\ 0 & 0 & 1 & -\frac{1}{2} & -1 & \frac{3}{2} \end{vmatrix} \begin{vmatrix} \nu_{SrAl_2Si_2O_8} \\ \nu_{Sr_2Al_2SiO_7} \\ \nu_{SrAl_2O_4} \\ \nu_{SiO_2} \\ \nu_{SrSiO_3} \\ \nu_{Al_2O_3} \end{vmatrix} = \begin{vmatrix} 0 \\ 0 \\ 0 \\ 0 \\ 0 \\ 0 \end{vmatrix} \tag{7}$$

The solution for independent reactions can be then calculated as follows:

$$SrAl_2Si_2O_8 \rightarrow SrAl_2O_4 + 2SiO_2 \quad \left[\nu_{SiO_2} = 1, \ \nu_{SrSiO_3} = 0 \text{ and } \nu_{Al_2O_3} = 0\right] \tag{8}$$

$$Sr_2Al_2SiO_7 \rightarrow SrAl_2O_4 + SrSiO_3 \quad \left[\nu_{SiO_2} = 0, \ \nu_{SrSiO_3} = 1 \text{ and } \nu_{Al_2O_3} = 0\right] \tag{9}$$

$$SrAl_2Si_2O_8 + 3SrAl_2O_4 \rightarrow 2Sr_2Al_2SiO_7 + 2Al_2O_3 \quad \left[\nu_{SiO_2} = 0, \ \nu_{SrSiO_3} = 0 \text{ and } \nu_{Al_2O_3} = 1\right] \tag{10}$$

The reaction thermodynamics for these three reactions was estimated via the HSC software and the results of standard reaction Gibbs energy are introduced in Table 2.

The fact that the formation of strontian via the reaction of single oxides and binary oxide intermediates according to Eqs. ((8)–10) is not preferred from the thermodynamic point of view provides the explanation for experimentally observed mechanism using the non-equilibrium melt. The three independent reactions are the formation of strontian, the formation of gehlenite and the transformation of gehlenite into strontian. This conclusion is in agreement with experimental results in Fig. 6(a).

### 3.3. Reaction kinetics and thermodynamics of activated state

Since strontian does not appear up to the temperature of 1150 °C and at the temperature of 1660 °C it is the only thermodynamically stable product of thermal treatment, the concentration of $SrAl_2Si_2O_8$ increases naturally from 0% to 100%. The degree of conversion ($\alpha = 100w_1, T/w_1, 1660$ °C) can be then directly calculated from the results of quantitative X-ray diffraction analysis (Fig. 6(b)). The model dependent technique (Eqs. (3) and (4)) enables to determine the kinetic function of $F_{2/3}$ (the kinetics of

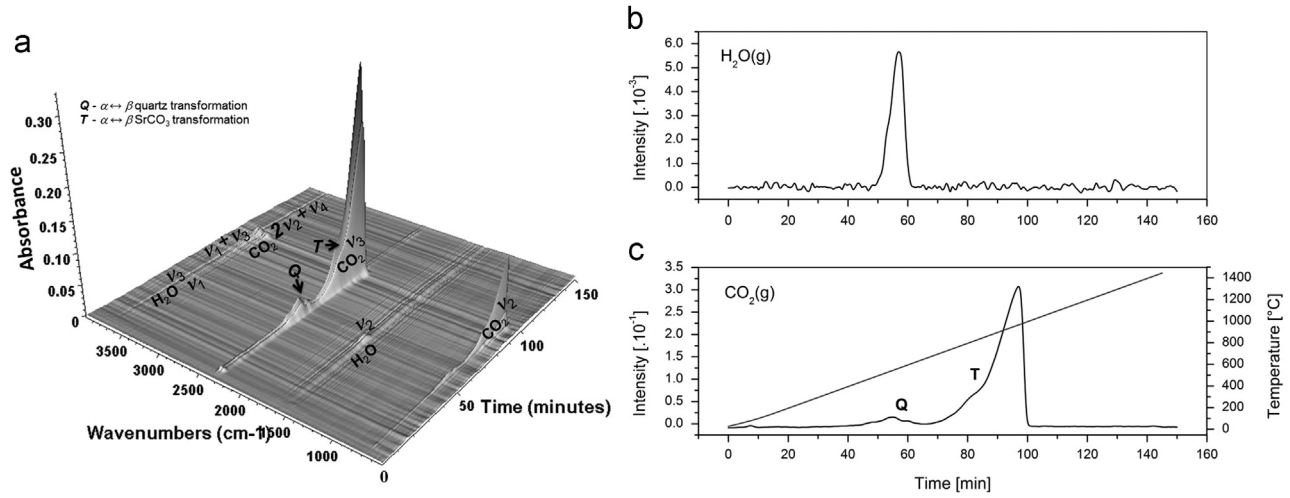


**Fig. 4.** EGA analysis of raw meal during the thermal treatment to 1450 °C (a) and time dependence of gaseous products released from the sample: water (b) and carbon dioxide (c).

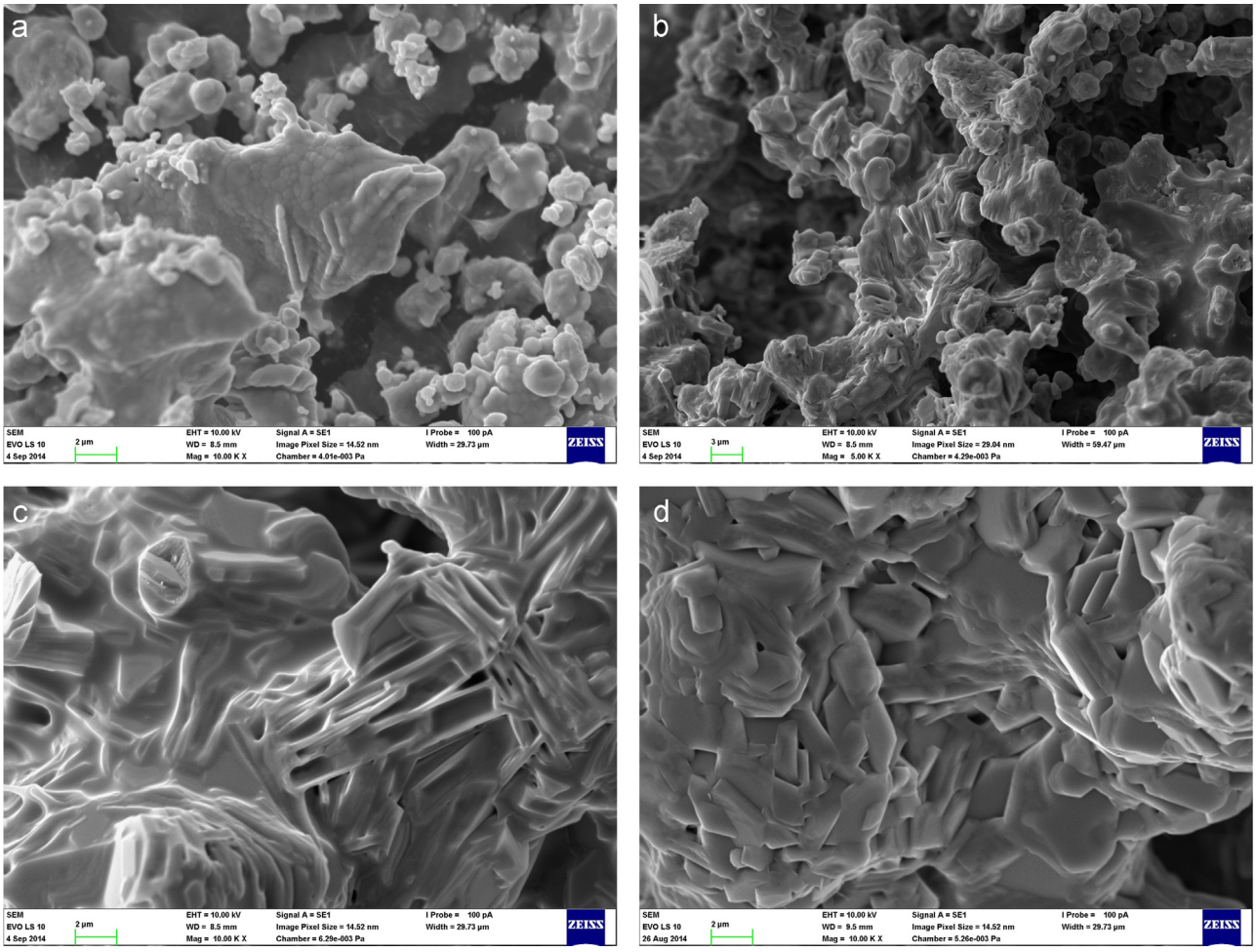


**Fig. 5.** SEM picture of strontian treated to the temperatures of 1150 °C (a), 1300 °C (b), 1400 °C (c) and 1660 °C (d).

chemical reaction of 3/2 order) as the most probable reaction mechanism of formation of strontian (Table 3) within the conversion interval ($\alpha$) from 5% to 95%.

The kinetic plots for integral and differential method are shown in Fig. 7(a). Determined kinetic data are listed in Table 4. Both methods identify the same kinetic function ($\boldsymbol{F}_{2/3}$) and the difference between determined values of apparent activation energy makes only about 3.7%. The reconstruction of the process using determined kinetic results is introduced in Fig. 7(b). Observed difference shows that the value of frequency factor is underestimated and overestimated for differential and integral method, respectively. Neverthless, the average kinetic data are in a good agreement with the course of synthesis of strontian via applied ceramic method.

The calculation of the transition-state thermodynamic functions of investigated process is based on the Eyring (or Eyring–Polanyi) equation, which resembles the Arrhenius law [84,89] for the

temperature dependence of the rate constant ($k(T)$) [85–87,90]

$$k(T) = \kappa A \exp\left[-\frac{E_a}{RT}\right] = \kappa\frac{k_B T}{h}\exp\left[\frac{\Delta S^{\#}}{R}\right]\exp\left[-\frac{\Delta H^{\#}}{RT}\right] = \kappa\nu \exp\left[-\frac{\Delta G^{\#}}{RT}\right] = \kappa\nu K^{\#} \quad (11)$$

where $k_B$, $h$ and $\nu = k_B T/h$ are the Boltzmann ($1.381 \times 10^{-23}$ J K$^{-1}$), the Planck ($6.626 \times 10^{-34}$ J s) constant and the vibration frequency, respectively. The values of transmission coefficient $\kappa$ are in many cases equal to unity [88,91]. The thermodynamic parameters of activated complex, including Gibbs free energy ($\Delta G^{\#}$), enthalpy ($\Delta H^{\#}$) and entropy ($\Delta S^{\#}$) of the process (initial state↔transition state [68,92]) were calculated using the relations [87,88,90]

$$\Delta H^{\#} = E_{ap} - RT \quad (12)$$

$$\Delta S^{\#} = R\left[\ln\left(\frac{hA}{k_B T}\right) - n\right] \quad [\kappa = 1] \quad (13)$$

where the reaction order $n$ is about 1.5 (Table 3) and

$$\Delta G^{\#} = \Delta H^{\#} - T\Delta S^{\#} \quad (14)$$

Calculated values of transition-state thermodynamic parameters are summarized in Table 4.

Assuming that both reactions are the same kinetics, Eq. (11) also provides the option to calculate the value of rate constant of the process at the temperature of 1300 and 1400 °C, i.e. for temperatures where $k_1/k_2$ ratios were determined (Table 1). This enables to calculate the reaction rate constant $k_2$ which is related to the formation of Sr-gehlenite. The results determined via both methods are introduced in Table 4.

## 4. Conclusion

The synthesis of feldspar strontian from raw meal composed of $SrCO_3$, $Al_2O_3$ and $SiO_2$ powders via the ceramic route proceeds at the temperature ≥ 1150 °C. The main reaction pathway is initiated by the thermal decomposition of $SrCO_3$, continues by the formation of binary oxide intermediates and primary strontian via the crystallization from non-equilibrium melt. Reactions between intermediates or the reaction of these intermediates with $SiO_2$ and $Al_2O_3$ lead to the formation of secondary strontian. The large plate-like particles of tertiary strontian were formed by recrystallization of primary and secondary strontian. Strontian becomes a single crystalline phase within the

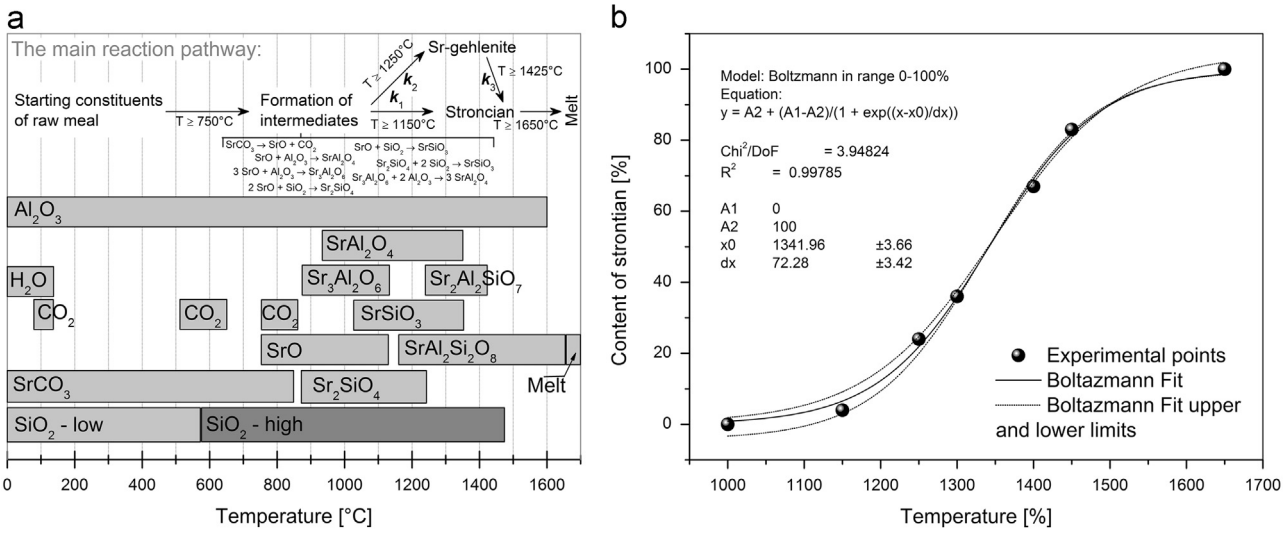


**Fig. 6.** The course of synthesis and the temperature range of stability of intermediates formed during the thermal treatment of raw meal (a) and the influence of temperature on the content of strontian (b).

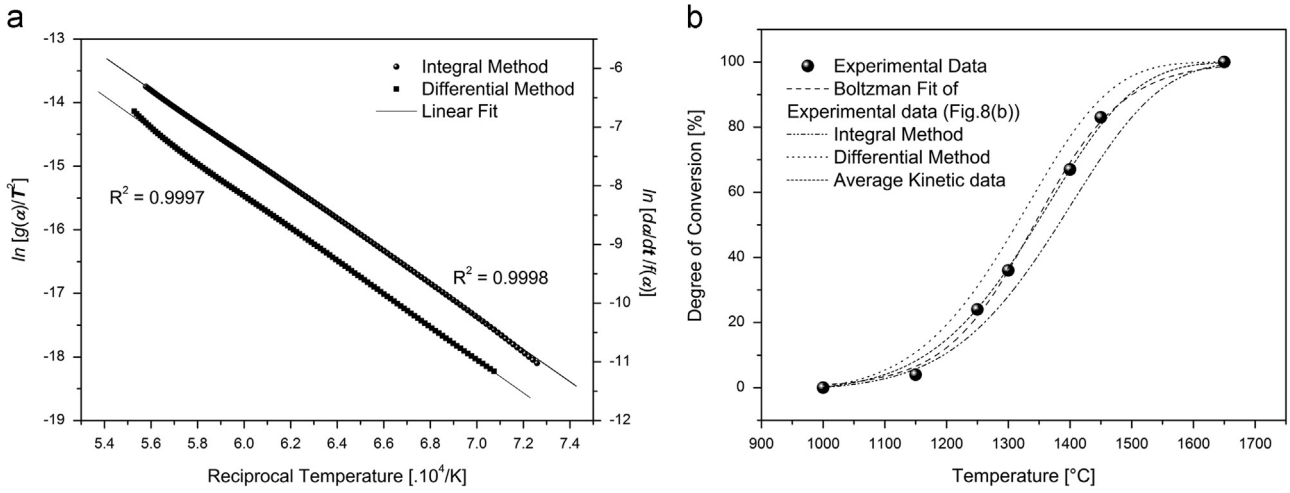


**Fig. 7.** Kinetic plots for integral and differential method (a) and the comparison of results calculated from assessed kinetic data with experiments (b).

**Table 4**
The overview of kinetic and thermodynamic parameters for activated state.

| Parameter | | Integral method | Differential method | Average |
|---|---|---|---|---|
| $E_{ap}$ | [kJ mol$^{-1}$] | 225.1 | 233.5 | 229.3 |
| $A$ | [s$^{-1}$] | $2.4 \cdot 10^5$ | $1.8 \cdot 10^5$ | $2.1 \cdot 10^5$ |
| $n$ | – | 1½ | 1½ | 1½ |
| $\Delta H^{\#}$ | [kJ mol$^{-1}$] | 211.9 ± 0.2 [1000–1650 °C] | 220.2 ± 0.2 [1000–1650 °C] | 216.0[a] |
| $\Delta S^{\#}$ | [J (mol K)$^{-1}$] | − 168.3 ± 0.1 [1000 − 1650 °C] | −170.7 ± 0.1 [1000 − 1 650 °C] | − 169.4[a] |
| $\Delta G^{\#}$ | [kJ mol$^{-1}$] | 480.8 ± 4.4 [1000 − 1650 °C] | 493.2 ± 4.5 [1000 − 1650 °C] | 486.9[a] |
| $k_{1,1300\ °C}$ | [s$^{-1}$(mol m$^{-3}$)$^{1-n}$][b] | $4.9 \cdot 10^{-3}$ | $1.9 \cdot 10^{-3}$ | $3.1 \cdot 10^{-3}$[a] |
| $k_{1,1400\ °C}$ | | $1.3 \cdot 10^{-2}$ | $5.6 \cdot 10^{-3}$ | $8.8 \cdot 10^{-3}$[a] |
| $k_{2,1300\ °C}$ | | $8.2 \cdot 10^{-4}$ | $3.2 \cdot 10^{-4}$ | $5.2 \cdot 10^{-4}$[a] |
| $k_{2,140\ °C}$ | | $1.3 \cdot 10^{-3}$ | $5.7 \cdot 10^{-4}$ | $8.8 \cdot 10^{-4}$[a] |

[a] The value was calculated from average data of apparent activation energy and frequency factor.
[b] As the dimension of rate constant depends on the reaction order $n$, the corresponding unit is [s $\sqrt{}$(mol m$^{-3}$)]$^{-1}$.

temperature range from 1600 °C to the melting point temperature at 1660 °C. The analysis of phase composition and the Gibbs stoichiometric rule reveal three independent reactions, which lead to two parallel reaction pathways. Strontian can be formed via more favored reaction of single and binary oxides ($k_1$) or via the route using Sr-gehlenite as the intermediate ($k_2$).

The rate of one and half order reaction ($n=1½$) was recognized as the most probable mechanism (kinetic function $F_{2/3}$:$(1-\alpha)^{-1/2}-1$) of synthesis of feldspar strontian by both, integral and differential method. The values of apparent activation energy for integral and differential method were determined to be 225.2 and 233.5 kJ mol$^{-1}$, respectively. The comparison of experimental results with the course of the process calculated from average values of apparent activation energy (229.3 kJ mol$^{-1}$) as well as frequency factor ($2.1 \times 10^5$ s$^{-1}$) provides a good agreement between those results. The average Gibbs free energy, enthalpy and entropy of activated complex were calculated to be 486.9 kJ mol$^{-1}$, 216.0 kJ mol$^{-1}$ and − 169.4 J (mol K)$^{-1}$, respectively.

## Acknowledgments

This work was supported by the Project no. CZ.1.05/2.1.00/01.0012 Materials Research Centre at FCH BUT supported by the Operational Program Research and Development for Innovations.

## References

[1] J.V. Smith, Feldspar Minerals: 2 Chemical and Textural Properties, Springer Science & Business Media, Berlin, Heidelberg, 1974.
[2] M.M. Krzmanc, B. Jančar, D. Suvorov, The influence of tetrahedral ordering on the microwave dielectric properties of $Sr_{0.05}Ba_{0.95}Al_2Si_2O_8$ and (M=Al, Ga, M′=Si, Ge) ceramics, J. Eur. Ceram. Soc. 28 (2008) 3141–3148.
[3] M. De Graef, M.E. McHenry, Structure of Materials: An Introduction to Crystallography, Diffraction and Symmetry, Cambridge University Press, Cambridge, 2007.
[4] D. Emery, A. Robinson, Applications to Petroleum Geology, John Wiley & Sons, New York, 2009.
[5] L.V. Pirsson, Petrography and geology of the igneous rocks of the highwood mountains, U.S. Geological Survey Bulletin, Montana, 1905.
[6] J.S. Diller, H.B. Patton, The Geology and Petrography of Crater Lake National Park, Series Geological Survey Professional Paper, 1902.
[7] E. El-Meliegy, R. van Noort, Glasses and Glass Ceramics for Medical Applications, Springer, New York, 2012.
[8] C.B. Carter, M.G. Norton, Ceramic Materials: Science and Engineering, Springer, New York, 2007.
[9] F. Singer, Industrial Ceramics, Springer, The Netherlands, 2013.
[10] A.O. Surendranathan, An Introduction to Ceramics and Refractories, Taylor & Francis, Boca Raton, FL, 2014.
[11] J.C. Fernández-Caliani, E. Galán, P. Aparicio, A. Miras, M.G. Márquez, Origin and geochemical evolution of the Nuevo Montecastelo kaolin deposit (Galicia, NW Spain), Appl. Clay Sci. 49 (2010) 91–97.
[12] A.Ed.A. Santos Jr., Dd.F. Rossetti, Origin of the Rio Capim Kaolin based on optical (petrographic and SEM) data, J. S. Am. Earth Sci. 26 (2008) 329–341.
[13] C.S. Ross, S.B. Hendricks, Minerals of the Montmorillonite Group: Their Origin and Relation to Soils and Clays, U.S. Goverment Printing Office, 1943.
[14] F. Bétard, L. Caner, Y. Gunnell, G. Bourgeon, Illite neoformation in plagioclase during weathering: evidence from semi-arid Northeast Brazil, Geoderma 152 (2009) 53–62.
[15] X. Wang, M. Zhang, W. Zhang, J. Wang, Y. Zhou, X. Song, T. Li, X. Li, H. Liu, L. Zhao, Occurrence and origins of minerals in mixed-layer illite/smectite-rich coals of the Late Permian age from the Changxing Mine, eastern Yunnan, China, Int. J. Coal Geol. 102 (2012) 26–34.
[16] C. Hecker, M van der Meijde, F.D. van der Meer, Thermal infrared spectroscopy on feldspars – successes, limitations and their implications for remote sensing, Earth Sci. Rev. 103 (2010) 60–70.
[17] A. Tripathi, J.B. Parise, Hydrothermal synthesis and structural characterization of the aluminogermanate analogues of JBW, montesommaite, analcime and paracelsian, Microporous Mesoporous Mater. 52 (2002) 65–78.
[18] R.A. McCauley, Polymorphism and dielectric electric properties of Ba- and Sr-containing feldspars, J. Mater. Sci. 35 (2000) 3939–3942.
[19] G.H. Donnay, Hexagonal $CaAl_2Si_2O_8$, Acta Crystallogr. 5 (1952) 153.
[20] P. Ptáček, T. Opravil, F. Šoukal, J. Havlica, R. Holešinský, Kinetics and mechanism of formation of gehlenite, Al–Si spinel and anorthite from the mixture of kaolinite and calcite, Solid State Sci. 26 (2013) 53–58.
[21] S. Kurama, E. Ozel, The influence of different CaO source in the production of anorthite ceramics, Ceram. Int. 35 (2009) 827–830.
[22] K. Traoré, T.S. Kabré, P. Blanchart, Gehlenite and anorthite crystallisation from kaolinite and calcite mix, Ceram. Int. 29 (2003) 377–383.
[23] L. Barbeeri, A.B. Corradi, C. Leonelli, T. Manfredini, M. Romagnoli, C. Siligardi, The microstructure and mechanical properties of sintered celsian and strontium-celsian glass-ceramics, Mater. Res. Bull. 30 (1995) 27–41.
[24] Y.-M. Sung, S. Kim, Sintering and crystallization of off-stoichiometric $SrO \cdot Al_2O_3 \cdot 2SiO_2$ glasses, J. Mater. Sci. 35 (2000) 4293–4299.
[25] Y.-P. Fu, C.-C. Chang, C.-H. Lin, T.-S. Chin, Solid-state synthesis of ceramics in the BaO–SrO–$Al_2O_3$–$SiO_2$ system, Ceram. Int. 30 (2004) 41–45.
[26] C.E. Semler, W.R. Foster, Studies in the system $BaO-Al_2O_3-SiO_2$: VI, the system celsian-silica-alumina, J. Am. Ceram. Soc. 53 (1970) 595–598.
[27] B. Yoshiki, K. Matsumoto, High-temperature modification of barium feldspar, J. Am. Ceram. Soc. 34 (1951) 283–286.
[28] C. Ferone, B. Liguori, A. Marocco, S. Anaclerio, M. Pansini, C. Colella, Monoclinic (Ba, Sr)-celsian by thermal treatment of (Ba, Sr)-exchanged zeolite A, Microporous Mesoporous Mater. 134 (2010) 65–71.
[29] Y. Kobayashi, M. Inagaki, Preparation of reactive Sr-celsian powders by solid-state reaction and their sintering, J. Eur. Ceram. Soc. 24 (2004) 399–404.
[30] A. Marocco, B. Liguori, G. Dell'Agli, M. Pansini, Sintering behaviour of celsian based ceramics obtained from the thermal conversion of (Ba, Sr)-exchanged zeolite A, J. Eur. Ceram. Soc. 31 (2011) 1965–1973.
[31] N.P. Bansal, J.A. Setlock, Fabrication of fiber-reinforced celsian matrix composites, Compos. Part A: Appl. Sci. Manuf. 32 (2001) 1021–1029.
[32] W. Lei, R. Ang, X.-C. Wang, W.-Z. Lu, Phase evolution and near-zero shrinkage in $BaAl_2Si_2O_8$ low-permittivity microwave dielectric ceramics, Mater. Res. Bull. 50 (2014) 235–239.
[33] N. Fréty, A. Taylor, M.H. Lewis, Microstructure and crystallisation behaviour of sol–gel derived $1/2SrO \cdot 1/2BaO \cdot Al_2O_3 \cdot 2SiO_2$ glass-ceramic, J. Non-Cryst. Solids 195 (1996) 28–37.
[34] M.F.M. Zawrah, N.M. Khalil, Preparation and characterization of barium containing refractory materials, Ceram. Int. 27 (2001) 309–314.
[35] M. Chen, W.E. Lee, P.F. James, Synthesis of monoclinic celsian glass-ceramic from alkoxides, J. Non-Cryst. Solids 147–148 (1992) 532–536.
[36] A.S. Radosavljević-Mihajlović, M.D. Prekajski, J. Zagorac, A.M. Došen, S. S. Nenadović, B.Z. Matović, Preparation, structural and microstructural properties of $Ba_{0.64}Ca_{0.32}Al_2Si_2O_8$ ceramics phase, Ceram. Int. 38 (2012) 2347–2354.
[37] L.A. Orlova, N.V. Popovich, N.E. Uvarova, A. Paleari, P.D. Sarkisov, High-temperature resistant glass-ceramics based on Sr-anorthite and tialite phases, Ceram. Int. 38 (2012) 6629–6634.
[38] F. Clabau, A. Garcia, P. Bonville, D. Gonbeau, T. Le Mercier, P. Deniard, S. Jobic, Fluorescence and phosphorescence properties of the low temperature forms

of the $MAl_2Si_2O_8:Eu^{2+}$ (M=Ca, Sr, Ba) compounds, J. Solid State Chem. 181 (2008) 1456–1461.
[39] S. Ye, Z.-S. Liu, X.-T. Wang, J.-G. Wang, L.-X. Wang, X.-P. Jing, Emission properties of $Eu^{2+}$, $Mn^{2+}$ in $MAl_2Si_2O_8$ (M=Sr, Ba), J. Lumin. 129 (2009) 50–54.
[40] X. Zheng, Q. Fei, Z. Mao, Y. Liu, Y. Cai, Q. Lu, H. Tian, D. Wang, Incorporation of Si-N inducing white light of $SrAl_2Si_2O_8:Eu^{2+}$, $Mn^{2+}$ phosphor for white light emitting diodes, J. Rare Earths 29 (2011) 522–526.
[41] X. Yu, X. Xu, T. Jiang, H. Yu, P. Yang, Q. Jiao, J. Qiu, Tunable color emitting of $CaAl_2Si_2O_8$:Eu, Tb phosphors for light emitting diodes based on energy transfer, Mater. Chem. Phys. 139 (2013) 314–318.
[42] X. Yu, X. Xu, P. Yang, Z. Yang, Z. Song, D. Zhou, Z. Yin, Q. Jiao, J. Qiu, Photoluminescence properties and the self-reduction process of $CaAl_2Si_2O_8$:Eu phosphor, Mater. Res. Bull. 47 (2012) 117–120.
[43] M. Ma, D. Zhu, C. Zhao, T. Han, S. Cao, M. Tu, Effect of $Sr^{2+}$-doping on structure and luminescence properties of $BaAl_2Si_2O_8:Eu^{2+}$ phosphors, Opt. Commun. 285 (2012) 665–668.
[44] V.B. Pawade, N.S. Dhoble, S.J. Dhoble, Rare earth ($Eu^{2+}$,$Ce^{3+}$) activated $BaAl_2Si_2O_8$ blue emitting phosphor, J. Rare Earths 32 (2014) 593–597.
[45] D. Long-González, J. López-Cuevas, C.A. Gutiérrez-Chavarría, P. Pena, C. Baudin, X. Turrillas, Synthesis of monoclinic celsian from coal fly ash by using a one-step solid-state reaction process, Ceram. Int. 36 (2010) 661–672.
[46] B. Liguori, C. Ferone, S. Anaclerio, C. Colella, Monoclinic Sr-celsian by thermal treatment of Sr-exchanged zeolite A, LTA-type framework, Solid State Ion. 179 (2008) 2358–2364.
[47] H.D. Grundy, J. Ito, The refinement of the crystal structure of a synthetic non-stoichiometric Sr feldspar, Am. Mineral. 59 (1974) 1319–1326.
[48] G. Chiari, M. Calleri, E. Bruno, P.H. Ribbe, The structure of partially disordered, synthetic strontium feldspar, Am. Mineral. 60 (1975) 1319–1326.
[49] P.S. Dear, Sub-liquidus Equilibria for the Ternary System $SrO–Al_2O_3–SiO_2$, Virginia Polytechnic Institute, Blacksburg, 1957.
[50] P. Ptáček, Strontium Aluminate-Cement Fundamentals, Manufacturing, Hydration, Setting Behaviour and Applications, InTech Europe, Rijeka, Croatia, 2014.
[51] C.M. López-Badillo, J. López-Cuevas, C.A. Gutiérrez-Chavarría, J.L. Rodríguez-Galicia, M.I. Pech-Canul, Synthesis and characterization of $BaAl_2Si_2O_8$ using mechanically activated precursor mixtures containing coal fly ash, J. Eur. Ceram. Soc. 33 (2013) 3287–3300.
[52] A. Marocco, G. Dell'Agli, S. Esposito, M. Pansini, The role of residual $Na^+$ and $Li^+$ on the thermal transformation of Ba-exchanged zeolite A, Solid State Sci. 13 (2011) 1143–1151.
[53] V. Dondur, R. Dimitrijević, A. Kremenović, L. Damjanović, N. Romčević, S. Macura, The lithium- and sodium-enhanced transformation of Ba-exchanged zeolite LTA into celsian phase, J. Phys. Chem. Solids 69 (2008) 2827–2832.
[54] I. Lee, J. Covino, Sol-gel synthesis of monoclinic phase of barium aluminosilicate ceramics, Mater. Res. Bull. 29 (1994) 55–62.
[55] S. Bošković, Đ. Kosanović, D. Bahloul-Hourlier, P. Thomas, S.J. Kiss, Formation of celsian from mechanically activated $BaCO_3–Al_2O_3–SiO_2$ mixtures, J. Alloy. Compd. 290 (1999) 230–235.
[56] W. Franke, H. Ghobarkar, R.B. Heimann, The morphology of hydrothermally grown strontium paracelsian, J. Cryst. Growth 46 (1979) 474–478.
[57] C. Ferone, S. Esposito, M. Pansini, Microwave assisted hydrothermal conversion of Ba-exchanged zeolite A into metastable paracelsian, Microporous Mesoporous Mater. 96 (2006) 9–13.
[58] C.F. Dickinson, G.R. Heal, A review of the ICTAC Kinetics Project, 2000: Part 1. Isothermal results, Thermochim. Acta 494 (2009) 1–14.
[59] A. Tiwari, B. Raj, Reactions and Mechanisms in Thermal Analysis of Advanced Materials, Wiley, 2015.
[60] J. Cai, R. Liu, Kinetic analysis of solid-state reactions: a general empirical kinetic model, Ind. Eng. Chem. Res. 48 (2009) 3249–3253.
[61] P. Ptáček, M. Nosková, J. Brandštetr, F. Šoukal, T. Opravil, Mechanism and kinetics of wollastonite fibre dissolution in the aqueous solution of acetic acid, Powder Technol. 206 (2011) 338–344.
[62] J.B. Holt, I.B. Cutler, M.E. Wadsworth, Rate of thermal dehydration of kaolinite in vacuum, J. Am. Ceram. Soc. 45 (1962) 133–136.
[63] A.N. Kolmogorov, Selected Works of A.N. Kolmogorov: Mathematics and Mechanics, Springer, 1992.
[64] W.A. Johnson, R.F. Mehl, Reaction kinetics in processes of nucleation and growth, Trans. Metall. Soc. AIME 135 (1939) 416–441.
[65] M. Avrami, Kinetics of phase change. I General theory, J. Chem. Phys. 7 (1939) 1103–1112.
[66] N. Lazarevic, B. Adnadjevic, J. Jovanovic, Kinetic analysis of nicotine desorption from silicon dioxide under non-isothermal conditions, Thermochim. Acta 589 (2014) 100–106.
[67] G. Valensi, Kinetics of oxidation of metallic spherules and powders, Proc. USSR Acad. Sci. 202 (1926).
[68] V.F. Zhuravlev, I.G. Lesokhin, R.G. Tempelman, Kinetics in the formation of calcium aluminates and the role of mineralizers, Russ. J. Appl. Chem. 21 (1948) 887–902.
[69] C. Wagner, K. Grunewald, An article on the theory of the start-up procedure, Z. Phys. Chem. Abteilung B 40 (1938).
[70] C. Wagner, Ionen und elektronenleitung in silberbromid und abweichungen von der idealen stochiometrischen zusammensetzung, Z. Elektrochem. 63 (1959).
[71] E.G. Prout, F.C. Tompkins, The thermal decomposition of potassium permanganate, Trans. Faraday Soc. 40 (1944) 488–498.
[72] M.E. Brown, D. Dollimore, A.K. Galwey, Reactions in the Solid State Comprehensive Chemical Kinetics, Elsevier, Amsterdam, 1980.
[73] R. Riedel, I.W. Chen, Ceramics Science and Technology: Volume 1: Structures, John Wiley & Sons, 2008.
[74] C. Klein, A. Philpotts, Earth Materials: Introduction to Mineralogy and Petrology, Cambridge University Press, Cambridge, 2012.
[75] W. Borchardt-Ott, Crystallography, Springer, Berlin, Heidelberg, 1995.
[76] R. Dinescu, M. Preda, Thermal decomposition of strontium hydroxide, J. Therm. Anal. 5 (1973) 465–473.
[77] D. Inman, D.G. Lovering, Ionic Liquids, Springer, US, 2013.
[78] P. Ptáček, E. Bartoníčková, J. Švec, T. Opravil, F. Šoukal, F. Frajkorová, The kinetics and mechanism of thermal decomposition of $SrCO_3$ polymorphs, Ceram. Int. 41 (2015) 115–126.
[79] H.R. Wenk, A. Bulakh, Minerals: Their Constitution and Origin, Cambridge University Press, Cambridge, 2004.
[80] C.W. Hall, Laws and Models: Science, Engineering, and Technology, CRC Press, New York, 1999.
[81] R. Wegscheider, Über simultane Gleichgewichte und die Beziehungen zwischen Thermodynamik und Reactions kinetik homogener Systeme, Monatshefte Chem. 32 (1901) 849–906.
[82] G.S. Yablonskii, V.I. Bykov, V.I. Elokhin, A.N. Gorban, Kinetic Models of Catalytic Reactions, Elsevier Science, Amsterdam, 1991.
[83] J.D. Embury, High-temperature oxidation and sulphidation processes, in: Proceedings of the International Symposium on High-Temperature Oxidation and Sulphidation Processes, Elsevier Science, Hamilton, Ontario, Canada, August 26–30, 1990, 2013.
[84] W. Komatsu, T. Uemura, Kinetic equations of solid state reactions for counterdiffusion systems, Z. Phys. Chem. N. F. 72 (1970) 59.
[85] F. Kononiuk, Geterogennie Khimitceskie Reaktzii i Reaktzionnaia Sposobnosti, Nauka Tekh. (1945) 93.
[86] H.Y. Sohn, M.E. Wadsworth, Rate Processes of Extractive Metallurgy, Springer, US, 2013.
[87] W. Jander, Reaktionen im festen Zustande bei höheren Temperaturen. Reaktionsgeschwindigkeiten endotherm verlaufender Umsetzungen, Z. Anorg. Allg. Chem. 163 (1927) 1–30.
[88] A.M. Gistling, B.I. Brounshtein, Concerning the diffusion kinetics of reactions in spherical particles, J. Appl. Chem. USSR 23 (1950) 1327–1338.
[89] S. Arrhenius, P. pamphlets, Über die Dissociationswärme und den Einfluss der Temperatur auf den Dissociationsgrad der Elektrolyte, Wilhelm Engelmann, Leipzig, 1889.
[90] K.A. Connors, Chemical Kinetics: The Study of Reaction Rates in Solution, VCH, Weinheim, 1990.
[91] A.S. Wightman, N. Balazs, W. Kohn, Part I: Physical Chemistry. Part II: Solid State Physics, Springer, Berlin, Heidelberg, 2013.
[92] T.S.L. Radhika, T.K.V. Iyengar, T.R. Rani, Approximate Analytical Methods for Solving Ordinary Differential Equations, CRC Press, Boca Raton, FL, 2014.